IEEE Access
Multidisciplinary | Rapid Review | Open Access Journal

Received August 2, 2018, accepted August 28, 2018, date of publication September 5, 2018, date of current version September 28, 2018.

Digital Object Identifier 10.1109/ACCESS.2018.2868792

Optimal Heading Estimation Based Multidimensional Particle Filter for Pedestrian Indoor Positioning

LING PEI[1], DONGHUI LIU[1], DANPING ZOU[1], RONALD LEE FOOK CHOY[2], YUWEI CHEN[3], AND ZHE HE[4]

[1]Shanghai Key Laboratory of Navigation and Location-Based Services, School of Electronic Information and Electrical Engineering, Shanghai Jiao Tong University, Shanghai 200240, China
[2] Shanghai BeiDou Research Institute, Shanghai 201702, China
[3] Department of Remote Sensing and Photogrammetry, Finnish Geospatial Research Institute, 00521 Helsinki, Finland
[4] Appropolis Inc., Calgary, AB T2L 2A7, Canada

Corresponding author: Ling Pei (ling.pei@sjtu.edu.cn)

This work was supported in part by the National Nature Science Foundation of China under Grant 61873163 and in part by the Shanghai Science and Technology Committee under Grant 17DZ1100803.

ABSTRACT Localization capability is a challenging task in global navigation satellite system-degraded or denied environments. Alternatively, today's smartphones have an increased number of integrated sensors that can act as terminals for indoor personal positioning solutions such as pedestrian dead reckoning (PDR). However, magnetic interference, poor sensor measurements, and diverse handling of smartphone quickly decrease the performance for indoor PDR. This paper proposes a comprehensive and novel pedestrian indoor positioning solution in which heading estimation is improved by using simplified magnetometer calibration, by calculating projected acceleration along the moving direction using frequency-domain features and by applying direction constrains to indoor accessible paths. Moreover, compared with an ordinary particle filter (OPF) and a Kalman filter, this paper proposes a multidimensional particle filter (MPF) algorithm, namely MPF, which includes high-dimensional variables such as position, heading, step length parameters, motion label, lifetime, number of current particles, and factor. An MPF can handle more uncertain parameters than the OPF. Therefore, positioning with an MPF can achieve lower errors using low-quality sensors, mitigate interference introduced from surrounding environments, and reduce heading ambiguities due to different modes of carrying a smartphone. Consequently, field tests show that the proposed algorithm obtains robust performance for heading estimation and positioning.

INDEX TERMS Heading estimation, indoor positioning, particle filtering, pedestrian dead reckoning, smartphone localization.

I. INTRODUCTION

With widespread applications of Global Navigation Satellite System (GNSS), Location Based Services (LBS) have been widely applied outdoors. However, GNSS signals are degraded or denied for indoor environments due to signal attenuation and multipath effect. Therefore, in recent years one of the hottest research topics is to achieve reliable and accurate indoor navigation and positioning solution.

Since the increase in computational and sensing capabilities for commercial off-the-shelf (COTS) smartphones, we can observe a boost in emerging technologies, such as 3D mapping [1], AR/VR (Augmented Reality/Virtual Reality) [2], applied in personal LBS applications. Pedestrian Dead Reckoning (PDR) is an algorithm that uses accelerometer, gyroscope, and magnetometer sensors to calculate user's locations. Rich integrated sensors can enable smartphone-based PDR to become an alternative of indoor positioning methods [3], [4].

A PDR algorithm estimates the heading and step length from pedestrian gait information and calculate the current position of the pedestrian from the previous state [5]–[7]. Since PDR is a relative method, there will be an induced accumulated positioning error over time. Opportunistic signals, such as WiFi [8], Bluetooth [9], and magnetic field [10] can

provide absolute positioning in a certain range, but its popularity is limited by the deployment cost and signal database maintenance cost. Therefore, this paper proposes a solution using self-contained sensor data to form an indoor positioning system with optimal heading estimation and robust filter, which can significantly reduce the density of opportunistic signals and decrease the maintenance cost.

The heading estimation of PDR dominates the positioning accuracy and stability [11]. There is numerous research done related to the accuracy improvement of heading estimation. Most of them utilize magnetometer and gyroscope integrated into a custom Kalman filter to get optimized heading [12]–[15]. Moreover, [16] and [17] build weighted models to fuse the outputs from Inertial Measurement Unit (IMU). On one hand, some researches focus on heading estimation under different device carrying modes. On the other hand, some apply Principal Component Analysis (PCA) or enhanced PCA into heading estimation using data from accelerometer and gyroscope [18]–[22]. In the paper [23], the least-squares linear regression is used to calculate the direction of the horizontal acceleration to determine the walking direction. In this paper, an optimal heading estimation is achieved through three aspects: simplified sensor calibration, heading estimation using projected acceleration along a moving direction, and constrained current environment accessible path.

Based on the review of heading estimation, we can see that many researches utilize Kalman filter in pedestrian fusion positioning with multiple sensors and opportunistic signals [24], [25]. It is known that Kalman filter is the optimal filter for linear Gauss system [14]. However, in nonlinear PDR system with non-Gaussian noise, its performance will degrade. Therefore, there are researches using particle filter to optimize indoor positioning [26], [27]. But using ordinary particle filter (OPF) has a flaw such that it loses diversity of particles as the number of iterations increases.

Consequently, this paper proposes a robust modified particle filter algorithm namely Multidimensional Particle Filter (MPF). In an ordinary Particle Filter (OPF), each particle represents a possible 2D position and heading for the user in this PDR approach. Some positions are perhaps more likely than others, so each particle contains a weight value that represents the probability of it being correct based on all the information to date [26]. Unlike OPF, in a MPF, more uncertainties such as 2D coordinates, heading bias, step length parameters, motion state, particle lifetime, and so on, are assembled into a higher dimensional particle. The max number of particles varies with the number of walking steps and the density of walls. Based on the optimized particle filter, the performances of heading estimation and positioning are both improved.

In summary, our contributions of this paper include two parts:

Firstly, we propose a novel and comprehensive pedestrian indoor positioning solution in which heading estimation is improved by using a simplified magnetometer calibration, by calculating projected acceleration along moving direction using acceleration features in frequency domain, and by applying direction constrains to accessible paths instead of position constrains to free space.

Secondly, this paper proposes a high dimensional particle filter namely MPF which includes position, heading, step length parameters, motion label, lifetime, number of current particles, and factor which is a weight depending on external observations. MPF can handle more uncertain parameters compared to OPF. Therefore, positioning with a MPF can achieve lower errors using low quality sensors, mitigate interference introduced from surrounding environments, and reduce heading ambiguities due to different modes of carrying a smartphone.

This paper is structured as follows. The optimization of heading estimation is given in Sect. II; multidimensional particle filter positioning is presented in Sect. III; and final conclusion is drawn in Sect. IV.

II. THE OPTIMIZATION OF HEADING ESTIMATION

Heading in a PDR algorithm refers to the moving direction of a pedestrian. To obtain an accurate pedestrian heading is one of the major challenges in an indoor positioning system. On one hand, magnetometer is sensitive to metal objects and indoors electromagnetic interference. On the other hand, the accumulated heading drift is unavoidable if angulated integration is applied using gyroscope readings. Currently, the commonly used magnetometer calibration method is to rotate the smartphone around the figure ''8'' [28]. This methodology is time consuming due to the number of collected samples is generally not enough to calculate a valid calibration model, resulting in failures and reruns. Besides, the smartphone heading estimation is also influenced by the attitude or placement of the phone. Since the heading of PDR represents the walking direction of the pedestrian and not of the phone; any change in the phone placement during walking, calling or swinging phone in hand, will induce wrong moving direction. Some researches compensate the heading offset under different carrying modes by adding fixed heading bias [12], [29]. However, a large number of training samples from different people is needed to tune this set of heading bias in order to support diverse use cases.

To resolve the heading estimation issues addressed above, we firstly propose a simplified calibration method to optimize magnetometer calibration [36]. Then, a heading estimation algorithm using projected acceleration is introduced to reduce the influences by diverse phone placements. Finally, a constrain method is applied to generate a cleaner heading estimation from the accessible path.

A. THE CALIBRATION METHOD FOR SELF-CONTAINED MAGNETOMETER ON SMARTPHONE

Typical magnetometer reading is disrupted by external interference and internal errors [30], [31]. Internal errors of a magnetometer sensor caused by the manufacturing process

and components quality can be divided into non-orthogonal error, sensitivity error, sensor noise, and zero-offset [36].

Knowing the introduced error and analyzing the error criteria, we can obtain the error model equations of the magnetometer measurement system as follows [32]:

$$\tilde{\boldsymbol{B}} = \boldsymbol{\varepsilon}_{ni}(\boldsymbol{\varepsilon}_{nm}\boldsymbol{B}_c + \boldsymbol{\varepsilon}_{lm}) + \boldsymbol{\varepsilon}_{li} + \boldsymbol{\varepsilon}_w \tag{1}$$

where $\tilde{\boldsymbol{B}}$ is a vector consisting of three values measured from magnetic field. $\boldsymbol{B_c}$ represents real magnetic field vector; $\boldsymbol{\varepsilon}_{ni}$ is a 3-by-3 matrix representing nonlinear system errors including sensitivity error and non-orthogonal error; $\boldsymbol{\varepsilon}_{nm}$ is also a 3-by-3 matrix representing nonlinear error caused by magnetic interference, namely soft-iron effect; $\boldsymbol{\varepsilon}_{lm}$ is a vector representing linear error caused by magnetic perturbation, namely hard-iron effect; $\boldsymbol{\varepsilon}_{li}$ and $\boldsymbol{\varepsilon}_w$ represent zero-offset and sensor noise respectively.

After merging the similar items, we can get (2), the error model of magnetometer in this paper.

$$\tilde{\boldsymbol{B}} = \boldsymbol{A}\boldsymbol{B}_c + \boldsymbol{b} \tag{2}$$

in which $\boldsymbol{A}$ is a matrix representing multiplicative error and $\boldsymbol{b}$ represents linear errors.

After performing a magnetometer calibration, the magnetic field vector which we obtain should be equal to local geomagnetic vector. At this time, we rotate the smartphone randomly in the three-dimensional space to collect magnetic field data. The modulus of the data should be constant, and equal to the value of local geomagnetic field strength B [33]:

$$\boldsymbol{B}_c^T\boldsymbol{B}_c = B^2 \tag{3}$$

Combined with (2), we can get:

$$(\tilde{\boldsymbol{B}} - \boldsymbol{b})^T(\boldsymbol{A}^{-1})^T\boldsymbol{A}^{-1}(\tilde{\boldsymbol{B}} - \boldsymbol{b}) = B^2 \tag{4}$$

It is noted that the form of (4) is almost equivalent to the ellipsoid equation. Therefore, the errors of magnetometer are distributed on the surface of an ellipsoid. The centre of this ellipsoid depends on hard-iron effect $\boldsymbol{b}$, and the shape depends on the symmetric matrix $(A^{-1})^TA^{-1}$ [34]. The difference between the magnetic field vector before and after calibration is shown in Fig. 1.

If we collect enough magnetic field data and solve the ellipsoid equation of the distribution of magnetic vector, we can calculate $\boldsymbol{A}$ and $\boldsymbol{b}$ by matrix operation.

Moreover, if we compile the minimum data required for calibration purposes, we can design an efficient way to rotate the magnetometer in a smartphone which will collect a small quantity of magnetic field data with enough weight to fulfill our calibration process. With the body coordination system definition of smartphone as shown in Fig.2, we select two of three axes of the magnetometer in the smartphone as the rotational axes. Then we rotate smartphone around these two axes to collect data.

In principle, after we rotate the smartphone around one axis, we can roughly sketch the shape of the ellipsoid [36]. However just one circle of rotation cannot determine the

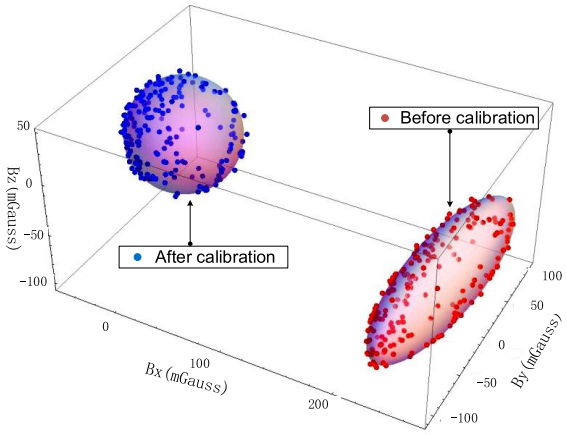

FIGURE 1. The comparison of magnetic field data before and after calibration [35].

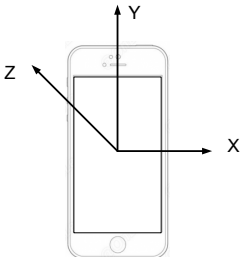

FIGURE 2. The body coordinate system of a smartphone.

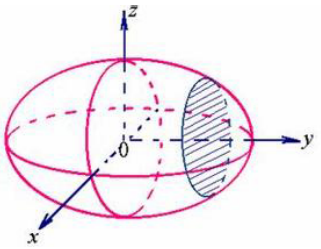

FIGURE 3. The shape of an ellipsoid.

equation as shown in Fig.3. Thus, we need to rotate the smartphone around another axis to get another trace on the surface of the ellipsoid. After we get two circles in two mutually perpendicular planes, we can determine the unique ellipsoid equation. Compared with other methods like six-directional stewing method [15], and ∞ shape method [28] this proposed technique requires fewer data and costs less time with the same calibration effect.

As collecting magnetic field data becomes more efficient, less time is spent on solving the ellipsoid equation calibration process. Therefore, we have specifically made a series of experiments and explored the cost effect to calibrate the smartphone based on different rotation modes.

All experiments were conducted in a typical office building. The sensors we used were embedded in a smartphone is AK8963 Magnetometer from Manufacturer AKM with

resolution of 0.15 μT/LSB and its sample rate is 100 Hz. The whole calibration process can be achieved both by online and offline. In this paper, we develop an indoor navigation App which performs the calibration process online.

First, magnetic field data were collected by rotating the smartphone around X and Z-axis of its coordinate system; quickly followed by the calibration output data. Some example data of our experiment are shown in Fig. 4 and Fig.5.

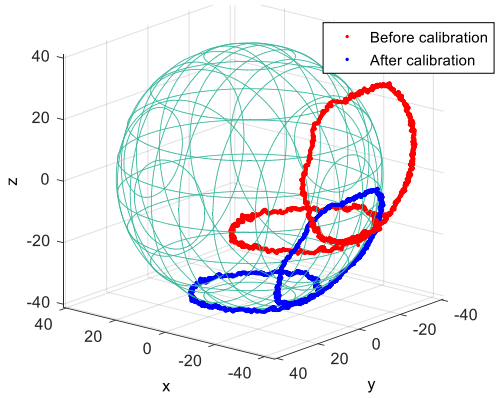

FIGURE 4. The distribution of magnetic field data before/after calibration. The red trace represents the data without calibration. The blue one is the result using calibration matrix proposed in this paper.

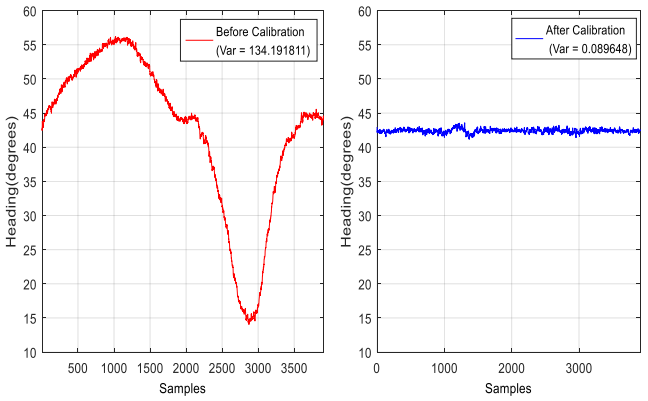

FIGURE 5. The readings of heading (the same data used in Fig. 4. The red line is the data before calibration. The blue line indicates the data after calibration).

The same data used in Fig.4 and Fig.5 is collected in a typical indoor environment. As shown in Fig.4, the trace after calibration is much closer to the light green sphere skeleton, which is equivalent to lower variance. Fig.5 demonstrates that after calibration the variance of the data is greatly reduced from 134.19 to 0.09 degrees.

Figure 6 is the experimental result of a 360-degree rotation in the horizontal plane using two similar smartphones at the same time.

This experiment was conducted by rotating two identical smartphones in horizontal plane for 360 degrees with a moto-drive rotation table which rotates with an even speed

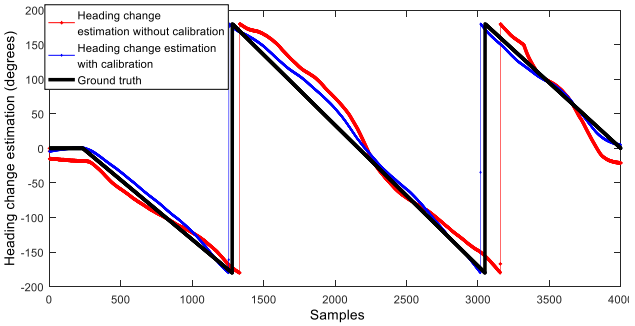

FIGURE 6. The heading change estimation results without and with calibration. This experiment was conducted by rotating two identical smartphones in horizontal plane for 360 degrees.

controlled by a computer. The ground truth was obtained from the computer of the rotation table. Compared with the results of heading change estimation with and without calibration, we can find that the heading change estimation with calibration is closer to the ground truth. The standard deviation of error is reduced from 19.50 to 8.80 degrees.

To verify the performance of the proposed algorithm, we have selected several representative methods to make comparison. The results are shown in Fig.7. Six-direction means taking the phone stewing in six different directions (usually direction of co-ordinate system). XYZ means rotating around the X, Y and Z-axis of the smartphone coordinate system respectively. XY means rotating around the X and Y-axis and so on. The experiments were taken both indoors and outdoors.

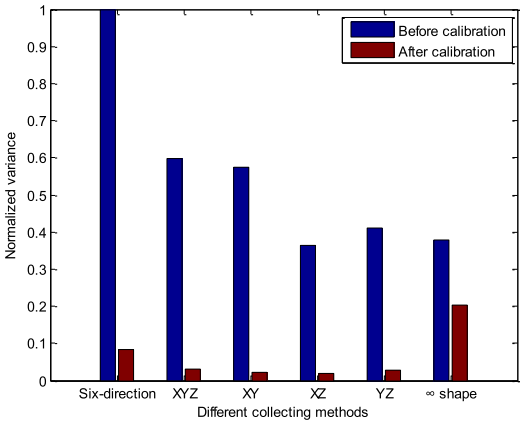

FIGURE 7. Variance of different methods of data collected indoors.

The result shows, the data variance applied with calibration using the proposed technique is reduced by 94.08% on average, while data collected by six-direction method is reduced by 91.73% and ∞ shape method by 49.83% averagely. Unlike six-direction method, the whole process of rotating phone around two axes of the phone takes only 2 to 4 seconds, while the former method needs at least 10 seconds to achieve the convergence criterion.

B. HEADING ESTIMATION BASED ON PROJECTED ACCELERATION ALONG MOVING DIRECTION

In this subsection, we propose a heading estimation algorithm using projected acceleration along pedestrian moving direction. The algorithm flow is summarized as Algorithm 1. In addition, subscript i in step 6 means the serial number of the steps detected by the step detection module and subscript j means the serial number of acceleration vector between the i-th step and the $(i+2)$-th step. The subscripts x, y mean the axes the data of acceleration vector respectively.

Algorithm 1 Heading Estimation Based on Projected Acceleration Along Moving Direction

1. **Data acquisition**: sample acceleration, angular rate and magnetic field vector at a fixed frequency. The acceleration is represented by $\boldsymbol{A}^b = \left[a_{x,b} \; a_{y,b} \; a_{z,b} \right]^T$
2. **Attitude calculation**: import the sensor data into AHRS to calculate the attitude of the smartphone relative to the reference coordinate system, and get the rotation matrix $\boldsymbol{C}_b^r$.
3. **Step detection**: input acceleration data into step detection module of PDR system to obtain the timestamp and walking frequency of each step event.
4. **Bandpass filtering**: do bandpass filtering for acceleration data to eliminate noise and other interference signals.
5. **Acceleration projection**: use $\boldsymbol{C}_b^r$ to project the filtered acceleration data into the reference frame.
$$\boldsymbol{A}^r = \boldsymbol{C}_b^r \boldsymbol{A}^b$$
6. **Integral computation**: integrate the processed acceleration in the time interval of adjacent step events according to the timestamp obtained from step 3.
$$\boldsymbol{S}_i^r = \sum_{step_i}^{step_{i+2}} \boldsymbol{A}_j^r$$
7. **Heading calculation**: get the heading by inverse trigonometric function.
$$\theta = \arctan \frac{S_x^r}{S_y^r}$$

AHRS (Attitude and Heading Reference System) is a system that can provide at least three Euler angles representing attitude including roll, pitch, and yaw, i.e. it can determine the attitude of the body relative to the reference system. MARG (Magnetic, Angular Rate and Gravity) is one of typical AHRS configurations, which consists of a three three-axis orthogonal accelerometer, gyroscope, and magnetometer. Usually, AHRS fuses data from MARG sensors to acquire the smartphone's attitude. In this paper, we adopted an AHRS algorithm from [38], which is a novel orientation filter with low computational load using a single adjustable parameter tuning associated with Kalman-based approaches. An optimized gradient descent algorithm is applied to enable performance at low sampling rates. Furthermore, a real-time magnetic distortion and gyroscope bias drift compensation algorithm is designed [37], [38].

Step detection is a module of PDR system, which uses acceleration information to detect whether a step event occurs, which has been widely studied [7], [12], [37]. In our approach, we can achieve an accuracy of 99% for step detection with different phone placements [37]. We also evaluate the step length model with 5 subjects and achieve an average error of 3 cm for each step length estimation.

In this algorithm, we assume that moving direction will introduce dominate acceleration except gravity. Viewing from the frequency domain, we consider the frequencies of acceleration which generate forward movement are components that can be used for heading estimation. The noises caused by low cost sensor measures or interferences such as frequency introduced by side movements should be eliminated. It is found from experiments that some low-frequency components and high-frequency ones would also influence the result of heading estimation [39]. Therefore, a bandpass filter is added to enhance the signal quality. To retain more valuable frequency components, we set the passband frequency to 1/2 step frequency; low cut-off frequency is 1/4 step frequency; high cut-off frequency is 5/4 step frequency. And the passband attenuation is less than 3dB; stopband attenuation is no less than 80dB. The step frequency is given by step detection module of PDR system.

On the problem of filter selection, we summarize the orders required by different filters to satisfy the filtering conditions as shown in Table 1.

TABLE 1. The comparison of orders of bandpass filters.

Type	Name	Orders
IIR	Elliptic	12
	Butterworth	40
	Chebyshev Type I	20
	Chebyshev Type II	20
FIR	Least-squares	500
	Kaiser Window	603
	Equiripple	304

Because the frequency component we need to extract is small and phase distortion won't influence the result of the integral, a linear phase applied on the FIR will not be necessary. Moreover, from the experience of our experiments, it takes at least four walking steps to obtain enough data for FFT (Fast Fourier Transform) processing. In order to get real-time result, it is impractical to use FFT algorithm on an input data stream. Thus, a IIR filter with relatively fewer orders is chosen to reduce computation.

Finally, we use a 12-order Elliptic IIR filter to process the acceleration information. The amplitude-frequency and the phase-frequency characteristic diagram are shown in Fig. 8.

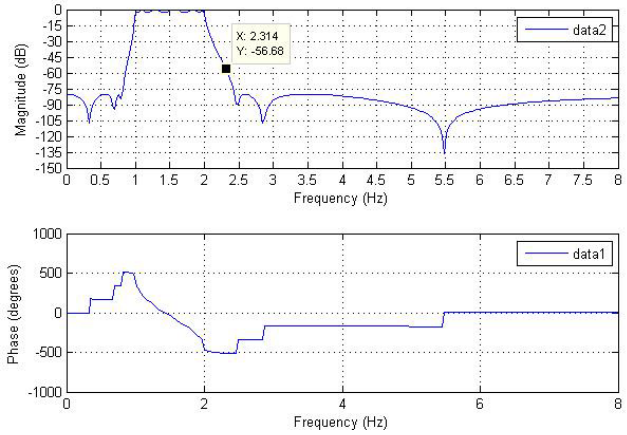

FIGURE 8. The amplitude-frequency and phase-frequency characteristic diagram of the bandpass filter.

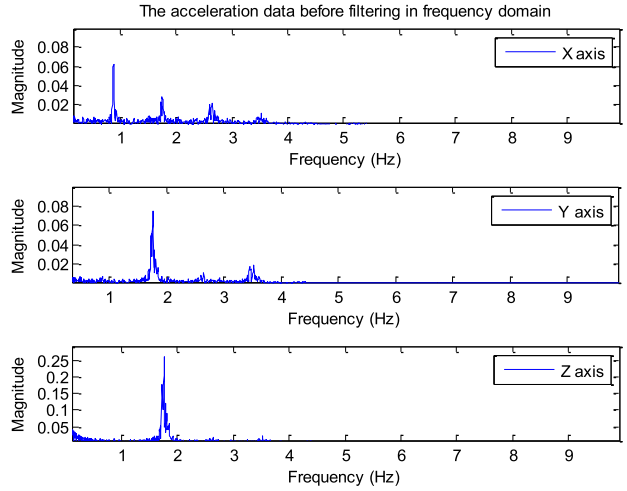

FIGURE 9. The raw acceleration data in frequency domain.

Fig.9 shows the waveform of raw acceleration data after FFT in frequency domain. The acceleration data were collected by a smartphone held as a texting message handling scenario, which means the Y-axis of sensor frame represents the moving direction of the pedestrian, and X-axis is perpendicular to the moving direction.

In Fig.9, we can find that the waveform on the axis representing the moving direction has the max peak near 2 Hz, which is almost equal to the step frequency of a human. Moreover, the waveform on the vertical axis to the moving direction has the max peak near 1 Hz, which is approximate to half of the step frequency of a human. When a pedestrian walk, his body will swing laterally, which is thought to be the main reason. The Fig.10 shows the filtered acceleration data in frequency domain.

As for the projection of acceleration, we use attitude angles from AHRS to build a coordinate transform matrix, then we can use this matrix to project sensor data from MARG into ENU (East-North-Up) frame by left multiplying the coordinate transform matrix.

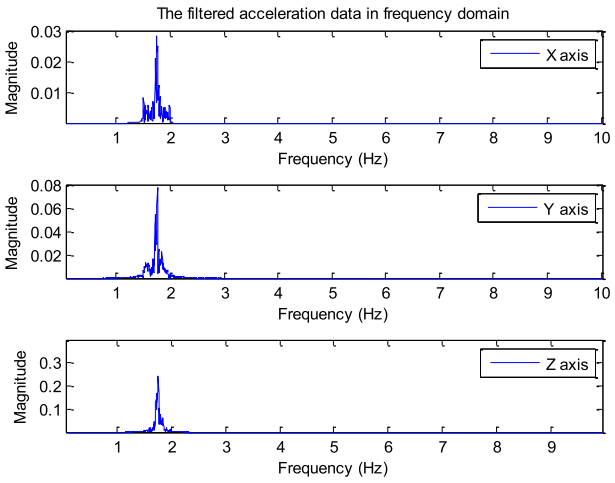

FIGURE 10. The filtered acceleration data in frequency domain.

From our experience, it's inaccurate to directly estimate heading from projected acceleration data in Step5 of Algorithm 1 due to the low quality of accelerometer embedded in smartphone and interference caused by excessive movement of human body. Moreover, it is unnecessary for a PDR system to constantly estimate the heading at all time. In fact, we only need to know the heading of each frequency step performed by the user so that we can calculate the current position from the previous one using dead reckoning method. Therefore, we propose to use the result of the integral acceleration to calculate the heading. To be more concrete, we use the integral acceleration data between every two steps, which would save computation time and eliminate the influence of the acceleration generated by the body's swinging motion during human walk.

We then apply arc cotangent function to calculate an angle from the integrated acceleration. The angle is regarded as the heading of the pedestrian. So far, we have achieved heading estimation. Combined with the results of step length estimation, the position and walking trajectory of the pedestrian can be calculated.

To verify the feasibility of this heading estimation method against varying phone placements, a series of experiments were carried out including handheld mode, photo mode, calling mode, and pocket mode as shown from Fig 11 (a)-(d) respectively [39]. The sample rate was set to 100Hz. Table 2 shows the information about the sensors and operating system of the smartphone utilized for testing. Set in a typical indoor office environment, a pedestrian carries a smartphone with each mode and walks along a corridor for two laps with a total length of about 100 meters. Table 3 shows that proposed algorithm can meet the requirements of heading estimation in PDR to some extent.

Wang *et al.* [29] proposed a context-based compensation solution which made a result of heading estimation with RMSE 2.56° in handheld mode, 7.58° in calling mode and 5.38° in pocket mode. Compared to the results of

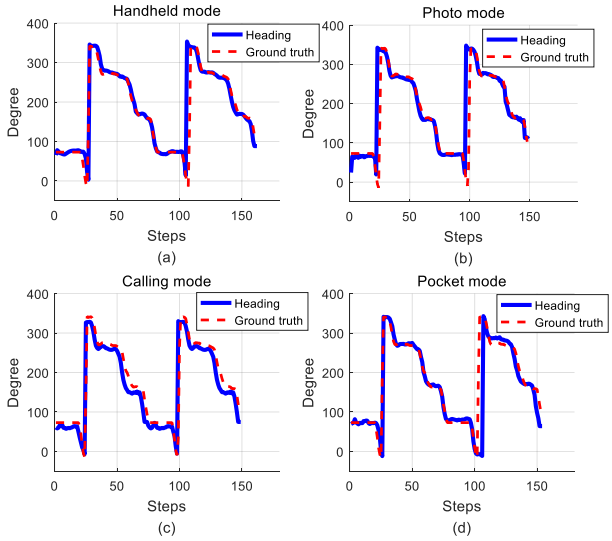

FIGURE 11. The results of heading estimation on handheld mode (a), photo mode (b), calling mode (c), and pocket mode (d).

TABLE 2. The description of smartphone used for testing.

Device Description	Specification
Name	Nexus 5
Operating System	Android 6.0.1 (32-bit)
Accelerometer	InvenSense MPU6515
Gyroscope	InvenSense MPU6515
Magnetometer	AKM AK8963
CPU	Snapdragon 800 (2.3GHz)
RAM	2GB

TABLE 3. Heading error analysis of Nexus 5 testing results.

Item	RMSE/Proposed	RMSE/[29]
Handheld mode	0.56°	2.56°
Photo mode	2.32°	-
Calling mode	8.48°	7.58°
Pocket mode	4.52°	5.38°

context-based compensation solution, the proposed method in this paper is much more accurate in handheld mode and pocket mode. The performance of calling mode is slightly worse. However, the compensation solution needs to detect the diverse contexts to compensate offset dynamically. The proposed method in this paper is more universal compared to the context-based compensation solution.

C. HEADING ESTIMATION BASED ON ACCESSIBLE PATH CONSTRAINTS

A priori map can provide constraints on the walking area given pedestrians normally walk in the accessible area of the map [37]. Furthermore, similar to map matching method applied to car navigation, this paper proposes a scheme to constrain pedestrians' heading by using map matching, that is, extract the valid open space area of the map to form accessible paths information including the setting direction of each road. This will assist heading estimation for our PDR system.

Different from the previous graph-based or link-node map matching solutions, we do not need to build the topological relationship for lines. The required structure of accessible path only includes the starting point and end point of each path and the direction of the path because the application of accessible path is mainly to assist the heading estimation.

There are also many existing algorithms for accessible path extraction [44]–[46]. In this paper, we use the widely applied indoor floorplan, such as Fig.12 (a) to generate the accessible path.

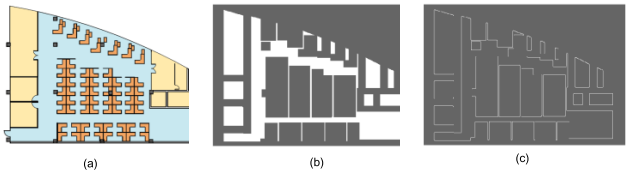

FIGURE 12. (a) The indoor map used in this project. (b) The accessible area obtained after image processing. The white area is the area we obtained. (c) The region boundaries (white lines) obtained by edge detection.

Therefore, only the accessible area is needed to be extracted from the indoor map, this will allow us to extrapolate the corresponding accessible path data.

This paper uses expansion and corrosion in digital image processing as the main strategy of road extraction. After processing, we can get the rough accessible area as shown in Fig.12 (b).

Next, we perform edge detection on the image shown in Fig.12 (b) with Canny operator. The edge image can be obtained as shown in Fig.12 (c).

After that, we use Hough Transform to extract the lines in the image, from which we can get the formula of each line in Fig.13 (a). Hough Transform is one of the basic image processing ways to identify geometric shapes. This method has been very effective for segmenting geometric shape with the same characteristics from the image.

We can find that there are numerous overlapping lines and very short lines in the set. Therefore, we are required to simplify and reduce the line set. The goal of the simplification is to remove the shorter line segments that overlap, and merge multiple segments to obtain a continuous line segment. After this simplification process is complete, we end up with the line set as shown in the following Fig.13 (b).

Now that we have defined the accessible path constraints for an indoor map, we can apply the accessible path into heading estimation assistance. We propose the following formula to assist heading estimation.

$$\theta_{final} = \frac{2\Delta\theta}{\pi}\theta_{compass} + \frac{\pi - 2\Delta\theta}{\pi}\theta_{R,i}$$
$$\Delta\theta = \min\left(\left|\theta_{compass} - \theta_{R,1}\right|, \left|\theta_{compass} - \theta_{R,2}\right|\right) \quad (5)$$

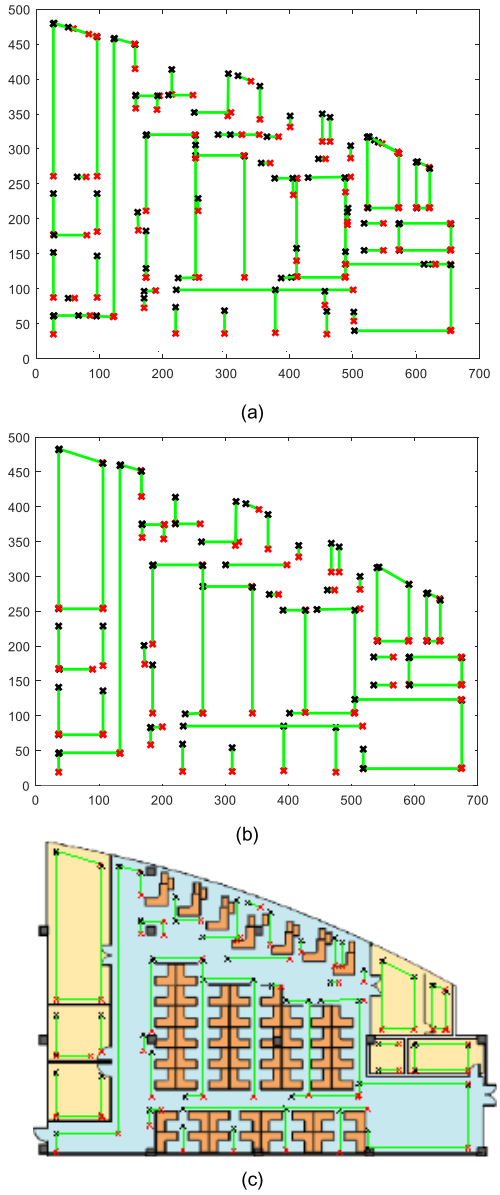

FIGURE 13. (a) The line set extracted by Hough Transform. (b) The simplified line set. (c) The accessible path of the indoor map.

where θ_{final} is the final result of heading estimation, and $\theta_{compass}$ is the heading calculated by a magnetometer or the smartphone in other ways. i can be 1 or 2, which depends on the source of $\Delta\theta$. This formula takes into consideration both the heading of road information and the randomness of a pedestrian walk. Moreover, in some areas like crossroads, a position may correspond to a number of roads. In that way, the calculation of $\Delta\theta$ can be extended to the following formula.

$$\Delta\theta = \min\left(\left|\theta_{compass} - \theta^i_{R,1}\right|, \left|\theta_{compass} - \theta^i_{R,2}\right|\right) \quad i \in \{n | d_n < threshold\} \tag{6}$$

where d_n is the distance between the pedestrian's position and n-th road, and $\theta^i_{R,1}$, $\theta^i_{R,2}$ are the directions of n-th road.

Because the accessible path assistance needs to be carried during pedestrian walking, we choose to hold a smartphone and walk around a fixed route to compare the difference between the heading and location with and without accessible path assistance. Specifically, the experimental environment is an ordinary office area. A tester holds the smartphone to keep the phone screen vertical and upward. The heading of the phone is consistent with the tester's direction. The route used for testing is shown in Fig. 14.

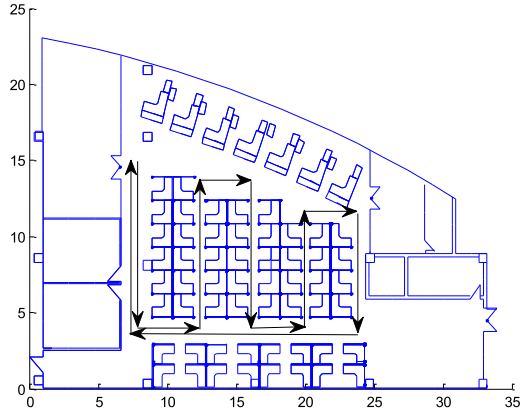

FIGURE 14. The diagram of accessible path assistance test walking route.

Fig. 15 shows the result of heading and positioning test without accessible path assistance, and Fig. 16 is the result of the test with accessible path assistance. We can find that the result of the simple PDR system is not ideal. We know the heading fluctuation is caused by the indoor magnetic field interference. Although the heading error is relatively small just by a few degrees, the long-term positioning accumulated effect would magnify this error.

TABLE 4. The positioning error of heading test about accessible path assistance.

Item	67th Error Percentile	95th Error Percentile
Without accessible path assistance	1.14m	2.96m
With accessible path assistance	0.53m	1.00m

The Table 4 is a statistics table of positioning error for the corresponding test using accessible path assistance. The test result using accessible path assistance demonstrates a significant improvement compared with the test result without accessible path. Moreover, we can clearly see the heading performance comparison in Fig. 17 and conclude that the heading estimation will be more stable with the added accessible path assistance.

III. MULTIDIMENSIONAL PARTICLE FILTER POSITIONING

Particle filter is a probability estimation algorithm based on the state of random particle approximation, which is suitable for solving problems in nonlinear non-Gaussian system.

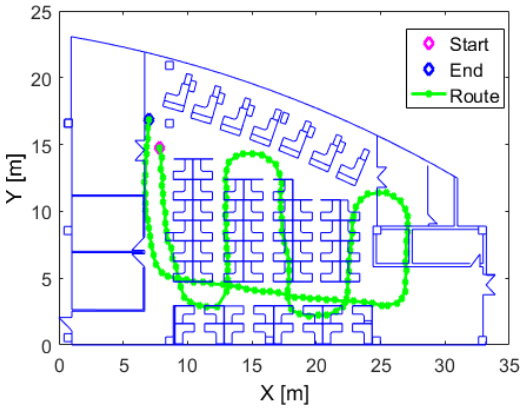

FIGURE 15. The result of heading and positioning tests without accessible path assistance.

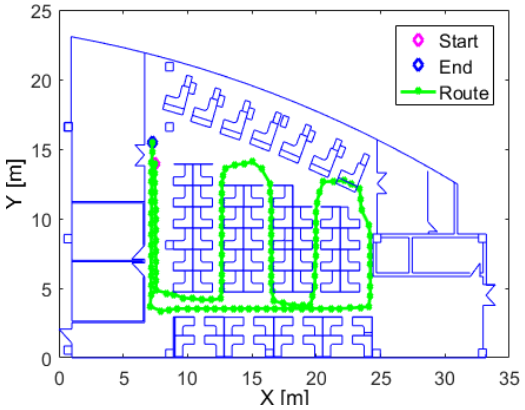

FIGURE 16. The result of heading and positioning test with accessible path assistance.

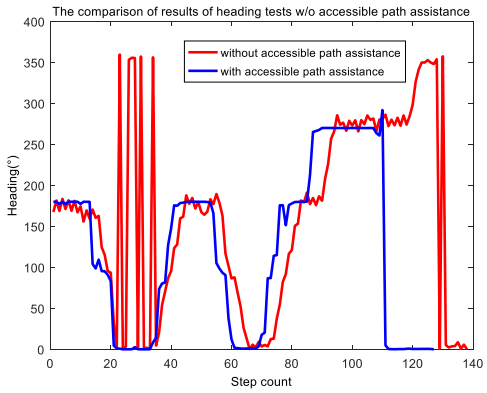

FIGURE 17. The comparison of results of heading tests with and without accessible path assistance. The X-axis is the step count during the test, and the Y-axis is the heading result in unit of degree. The red line is the result of the test without accessible path assistance, and the blue line is the one with accessible path assistance.

Therefore, it can be applied to a map constrained positioning system [47].

A. THE DESIGN OF PARTICLE FILTER

Generally, the flow of particle filter consists of several steps including prediction, update, normalization and resampling [48]. The core of resampling is to abandon the particles with smaller weights and clone the particles with larger weights [49].

The proposed multidimensional particle filter realizes indoor positioning by enriching the properties of the particles, optimizing the process, combining with motion recognition and opportunistic signal localization.

First, the motion model of the particle filter mainly propagates as the following equation (7).

$$\begin{cases} x_{k+1}^i = x_k^i + L_k^i \cdot \sin(\theta_k^i) \\ y_{k+1}^i = y_k^i + L_k^i \cdot \cos(\theta_k^i) \end{cases} \tag{7}$$

where x_k^i and y_k^i are the coordinates in north and east directions of the i-th particle at the step k, L_k^i and θ_k^i are the step length and heading of the i-th particle at step k.

$$\mathbf{Meas}_k = \{\mathbf{A}_k, \mathbf{G}_k, \mathbf{M}_k, \mathbf{O}_k\} \tag{8}$$

where the measurements at step k include the acceleration vector $\mathbf{A}_k$, gyroscope observations $\mathbf{G}_k$, magnetometer $\mathbf{M}_k$, and opportunistic signals $\mathbf{O}_k$.

The filter is driven by the step detection and the user's step event triggers a particle set resampling update. When a particle set update takes place, the filter would decide whether each particle is alive or dead based on the weight of the particle and wall collision detection. Walls are being represented as lines in the map. Particles are then added into corresponding particle set. The algorithm of collision detection refers to the existed algorithm [50]. The basic flow of the algorithm is shown in Fig. 18.

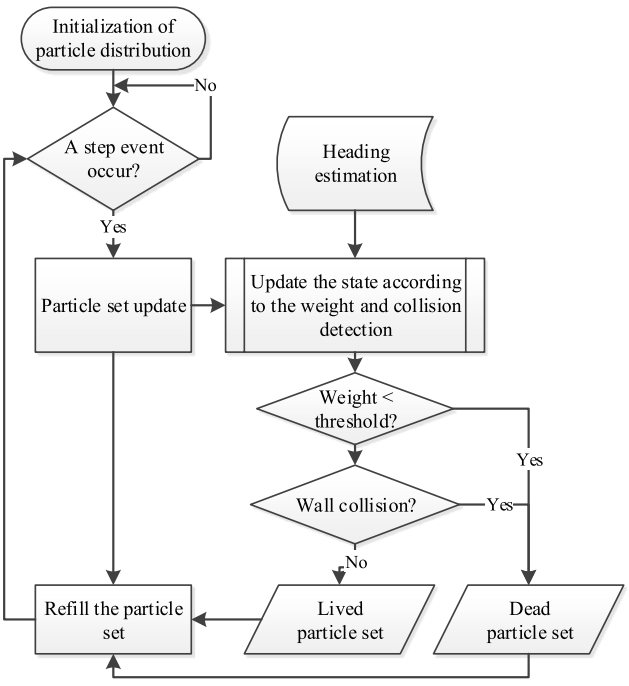

FIGURE 18. The flowchart of particle filter algorithm applied in indoor positioning.

Considering the possible states which might introduce positioning uncertainty, we design a high dimensional

particle filter. The variable states of the i-th particle at step k include position, heading, step length parameters, motion label, lifetime, number of current particles, and factor, i.e.

$$\mathbf{S}_k^i = \begin{pmatrix} \boldsymbol{P}_k^i & \theta_k^i & \boldsymbol{l}_k^i & m_k^i & t_k^i & n & c_k^i \end{pmatrix} \tag{9}$$

where $\boldsymbol{P}_k^i = \{x_k^i, y_k^i\}$, θ_k^i, $\boldsymbol{l}_k^i$ corresponds respectively to the 2D coordinates, heading, and step length parameters of the i-th particle, and m_k^i, t_k^i, c_k^i corresponds to the motion label, lifetime, and factor, n is the number of living particles. In our test we set the maximum number of living particles as 500 which ensures a promising result with an affordable computation for the test platform list at Table 2.

The states of pedestrian positioning include position coordinates, heading and step length parameters, from which the corresponding states of the particles can be sampled. The heading bias θ_k^i is given by a probability distribution when the particle is initialized. The step length model we used is a binary linear model associated with variance of step frequency and acceleration [37]:

$$L_k^i = \alpha_k^i \cdot Freq_k^i + \beta_k^i \cdot Var_k^i + \gamma_k^i \tag{10}$$

Therefore, the parameters of step length model are $\boldsymbol{l}_k^i = \begin{pmatrix} \alpha_k^i & \beta_k^i & \gamma_k^i \end{pmatrix}$.

The motion label m_k^i is designed for handling the heading bias caused by motion uncertainty. Different motion labels refer to different heading offset relative to walking direction. The heading offset can be calculated by the difference between the heading just before the motion changing and the one after changing, assuming people usually change carrying modes during walking straight lines. Motion label of the particle is assigned by motion recognition module according to the recognition probability, when the change of motion state is detected. The motion label assignment will be described in the follow-up sub-section.

Lifetime, t_k^i, is added to give a confidence to a living particle. Longer time a particle lives, higher confidence is given because we believe that the states of a particle with longer life are more reliable compared to the ones with short life. If a particle survives a long time, that is, it does not collide with the walls. It indicates that the particle attributes are similar to the real pedestrian states with a small margin of error.

Factor c_k^i is reserved for weighting particles given opportunistic signal observations $\mathbf{O}_k$ such as WiFi, Bluetooth, and so on. The particles closer to WiFi or Bluetooth positioning results will be given higher c_k^i.

The particle lifetime t_k^i and the particle factor c_k^i are both set to 1 at initialization. Every time a step event is detected, the lifetime is incremented by one up to a corresponding maximum threshold relative to the original value. The particle factor is assigned by a value between 0 to 1 depending on the range from the particle to the opportunistic signal positioning results. The weight of the particle ω_k^i is determined by the following expression:

$$\omega_k^i = c_k^i \cdot t_k^i \tag{11}$$

In the process of initialization, we add the zero mean Gaussian noise with the proper variance to the coordinates of each particle. Since the PDR system itself is unable to locate the initial position, there are two schemes presented in this paper for tabulating initial point positioning based on the PDR particle filter algorithm: one is user manual setting; the other is absolute opportunistic signal positioning localization. Moreover, to prevent "crossing walls" during positioning, we would make a collision detection between the surrounding walls against the line connecting the pedestrian coordinates and the particle coordinates. An example is shown in Fig. 19.

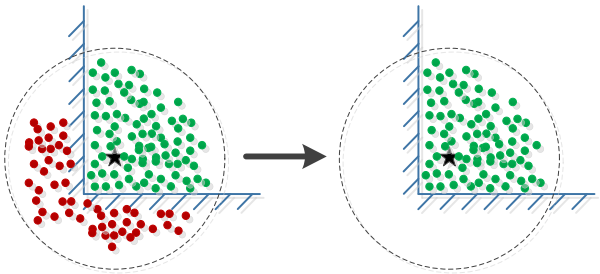

FIGURE 19. The diagram of optimized initialization distribution of particle filter. (Green dots: alive; Red dots: dead)

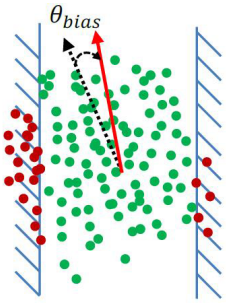

FIGURE 20. The diagram of particle filter correcting heading estimation. (Green dots: alive; Red dots: dead)

In Fig. 20, θ_{bias} represents the heading bias of the whole particle set, which can be calculated by (12).

$$\theta_{bias}^k = \frac{1}{N} \sum_i^N \theta_k^i \tag{12}$$

The heading bias θ_k^i of a particle is also initialized by zero-mean Gaussian distribution and θ_{bias} equals to zero. When the heading estimation performs badly in the process of positioning, some particles may die by colliding with the walls, which then allows us to abandon their heading biases. At this time, θ_{bias} is a non-zero value, which represents the difference between the true heading and the PDR system heading estimation.

If there is a step event detected by the PDR system, the filter will judge whether each particle is alive. The judgment conditions include map wall collision detection and weight threshold restriction. If a particle does not collide with any

walls or weighs higher than a certain threshold, that particle will be added into a live particle set and its lifetime will increase by one, or else it will be added into a dead particle set.

We also add a maximum divergence radius to eliminate particles too far from the particle set, which is shown in (13).

$$R_{\max} = c_3 \cdot e^{-c_4 \cdot N_{wall}} + R_{\min} \tag{13}$$

where $R_{\max}$ is the maximum divergence radius and c_3, c_4 are constant coefficients. N_{wall} is the number of wall lines around the position of a particle. $R_{\min}$ is the minimum divergence radius to ensure the most particles to be alive, which depends on the average width of the roads indoors which can be manually set.

When resampling the particles, the algorithm would sample the particles' attributes from the lived particle set, including the coordinates, the heading bias, the step length parameters and factor. The dead particle lifetime is initialized to one after having copied lived particle's attributes, of which the lifetime decreases by one. The dead particle maintains its number when copying attributes.

B. MOTION RECOGNITION ASSISTANCE

Most of PDR based smartphone indoor positioning systems utilize the heading of the smartphone to represent the heading of the pedestrian, which assumes that the pedestrian moving direction is same as the smartphone's heading. If the pedestrian rotates the phone in space for taking a photo or for calling, the phone heading estimation will also change even though the movement is kept in the same direction. This would introduce significant heading estimation errors for indoor positioning. Therefore, this paper uses motion recognition to assist particle filter to realize heading estimation and positioning under different phone carrying modes.

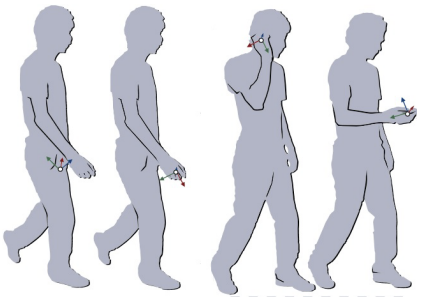

FIGURE 21. Four different modes of carrying a smartphone. From left to right: pocket, hand-swing, calling, handheld.

This paper optimizes four modes for carrying smartphones, as shown in Fig. 21, including handheld, calling, hand-swing, and pocket.

- Handheld mode: the pedestrian holds the smartphone to keep the screen upwards, and the phone's heading is aligned with the moving direction of the pedestrian.
- Calling mode: the pedestrian puts the phone near his ear, which leads to the misalignment between phone heading and moving direction.
- Hand-swing mode: the pedestrian holds the smartphone in his/her hand, swinging his/her arm around naturally during walking. Phone's heading changes with the hand swinging pattern.
- Pocket mode: the pedestrian put the phone in his/her pants pocket. Phone's heading changes with the body movement and constrains of the pocket.

Supervised learning algorithms such as decision tree and support vector machine, can be applied for detecting the carrying mode, also known as motion recognition. In the following description, we also use the word "motion" that has the same meaning as "carrying mode."

When a pedestrian moves along a straight line, his direction remains constant. At this time, for all four smartphone carrying modes, the direction of the pedestrian can be obtained through the phone yaw angle. There exists a simple linear relationship between all four carrying modes; therefore, we can extrapolate the moving direction just by using the smartphone yaw angle.

In this paper, the heading estimation adjustment is to compensate the direction deviation under different carrying modes by adding a corresponding angle bias $\Delta\theta_{motion}$. To be more concrete, we can record the headings for the past several steps. When a change and switch in motion state has been detected, the angle offset can be obtained by using the changed heading value and calculate the difference with the preserved value.

As for the hand-swing mode and pocket mode, the yaw angle is unstable when the pedestrian walks along a straight line. Therefore, this paper tries to find a pattern in the yaw angle change under these two modes.

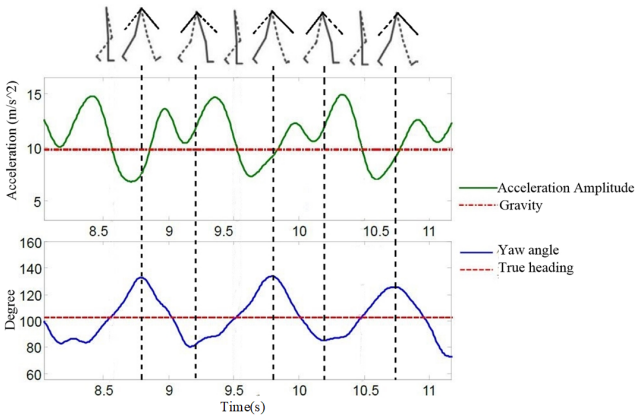

FIGURE 22. The variation of smartphone acceleration amplitude and yaw under hand-swing mode.

As shown in Fig.22, the acceleration amplitude curve and the yaw angle degree are characteristic to the human body's actual motion. On one hand, the amplitude is cyclical. On the other hand, we can correspond the extreme points of the yaw angle curve to the two pause points when a pedestrian performs an arm swinging motion. Thus this is the ideal time to compensate the angle offset during hand-swing mode and

pocket mode when the pedestrian' arm is placed at the two pause points.

Because the heading bias directly affects the heading estimation result, this paper recommends the system to save the headings of the past four steps during implementation, and only take the average of three values with the least variance as the heading θ_{before} before a carrying mode change occurs. At the same time, the average heading value of the two steps, after a carrying mode changes occurs, is stored as the output heading θ_{after}. We can get the heading bias by (14).

$$\Delta\theta_{motion} = \theta_{after} - \theta_{before} \tag{14}$$

However, the straight-forward compensation strategy is not robust enough to adapt to diverse scenarios. Therefore, we apply the multidimensional particle filter to improve the heading estimation robustness by introducing the motion label m_k variable which indicates the carrying mode.

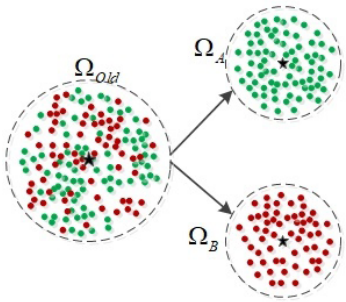

FIGURE 23. Particle assignment based on motion recognition result.

Each of the four carrying modes in this paper has the corresponding initial recognition probability. Assuming that the carrying mode probability after a motion changes occurs is defined as p_{motion}, as shown in Fig. 23, we would divide the lived particle set into the particle set Ω_A with the changed motion and the particle set Ω_B with original state according to the weight ratio $p_{motion} : (1 - p_{motion})$, and update corresponding motion label to the particles. Every motion label m_k has a corresponding recognition probability p_{motion}. And every time the mode changes, we think that there are only two possibilities of carrying modes, the original one and the new one. Therefore, we divide the whole particle set into two sets according to the particles motion labels.

In the update phase, two different particle sets are updated respectively according to the motion labels. For the particle set with changed motion, the new heading bias is calculated by equation (14), which would be used in particle update. If the weight ratio of one of two particle sets is lower than a certain threshold during positioning, this set will be eliminated and put into dead particle set.

The probability p_{motion} for each carrying mode would be initialized to 0.5 because the motion recognition using decision tree does not output the confidence probability. At the meantime, we would record the value of each probability in a local file when motion changes by equation (15).

$$p_{record} = 0.5 \cdot p'_{motion} + 0.5 \cdot p_{record} \tag{15}$$

where p_{record} is the recognition probability of the corresponding carrying mode in the local file, and p'_{motion} is the ratio of the weight of lived particles with corresponding carrying mode to the total weight. Moreover, p'_{motion} has an upper limit set as 0.9.

From using a multidimensional particle filter, we can get the filtered positioning result, and thus we can use this result to optimize PDR system heading estimation. As for the heading at every step event, we can take the heading estimation as a Markov process, given the heading at the subsequent step event is only related to the current step heading. Moreover, in most cases, a pedestrian will walk in a straight line when observing its positioning information. Therefore, the heading at last step is valuable for the current heading, in addition we can use the particle filter result to calculate the heading of the last step θ_{last} and use it to adjust the heading at the current step by (16).

$$\theta_{now} = \alpha \cdot \theta_{now} + (1 - \alpha) \cdot \theta_{last} \tag{16}$$

where α is a coefficient relative to the angular velocity modulus which, if necessary, can be manually set.

This heading adjustment is only available in the situation that the pedestrian is walking along a straight line. Therefore, we propose a judgment condition for turning as shown in equation (17).

$$\begin{cases} \sum\limits_{t-\tau<\delta} \|\boldsymbol{\omega}_\tau\| > threshold1 \\ |\theta_{now} - \theta_{last}| > threshold2 \end{cases} \tag{17}$$

where t is the current moment, and $\boldsymbol{\omega}_\tau$ represents the angular velocity at time τ.

If the condition (17) is satisfied, the pedestrian is most likely to turn a corner. In this case, α in equation (16) is set as 1, which means the heading estimation from last step cannot used for optimizing the current heading estimation.

C. FIELD TEST

First, we carried out a positioning test applied with multidimensional particle filter.

A tester walked along the path shown in Fig.24 (a) with the smartphone in handheld mode. Fig.24 (b) shows the heat map of local magnetic field strength. Red area is covered with strong magnetic field strength. Blue area indicates a weak magnetic field strength coverage. The test area is a typical magnetic field disturbed environment where the magnetic field strength is varying from 32.168uT to 52.244uT due to existing computers, GNSS receivers and simulators, micro oven, LED display, printer, concrete structure, and so on. In the process, the user changed the smartphone placement into calling mode, hand-swing mode and pocket mode for each walking circle. The total length of each walking cycle is about 300 meters. The result is shown in the Fig.25.

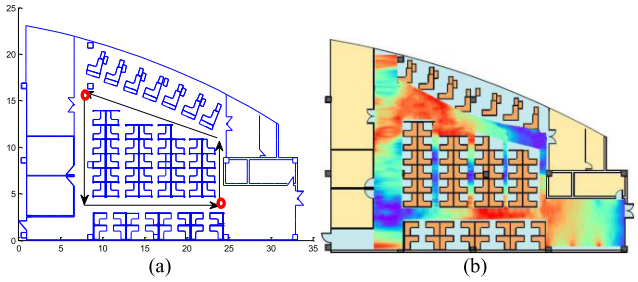

FIGURE 24. (a) The path of indoor positioning test. Red circles mean the positions of Bluetooth beacons for initial localization. Black arrows show the directions of the test path. (b) The strength heat map of magnetic field in the test area. Red area is covered with strong magnetic field strength. Blue area indicates a weak magnetic field strength coverage.

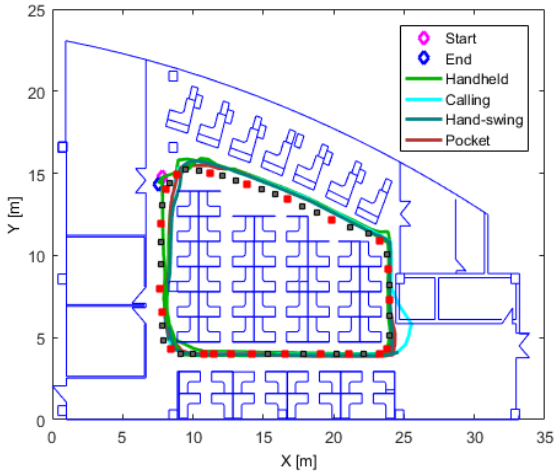

FIGURE 25. Indoor positioning result of multidimensional Particle Filter. The red and black solid blocks are the reference points for positioning. The handheld mode corresponds to the light green trajectory; the calling mode corresponds to the bright blue trajectory; the hand-swing mode and the pocket mode correspond to the dark blue and red trajectories respectively. The start and end points are the same for all trajectories.

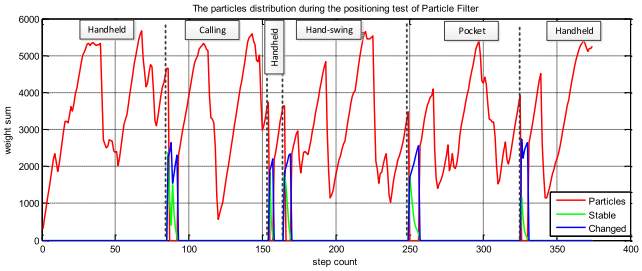

FIGURE 26. The particle distribution during the positioning test of particle filter. The red curve is the weight sum change of the old particle set. The blue curve shows the weight sum change of the particle set after motion changed. The green curve shows the weight sum change of the particle set remaining previous motion.

At the same time, we give a schematic particle distribution diagram in the process for this test as shown in Fig.26.

Moreover, we made a positioning performance comparison test using ordinary particle filter (OPF), and also Kalman filter (KF) under different carrying modes.

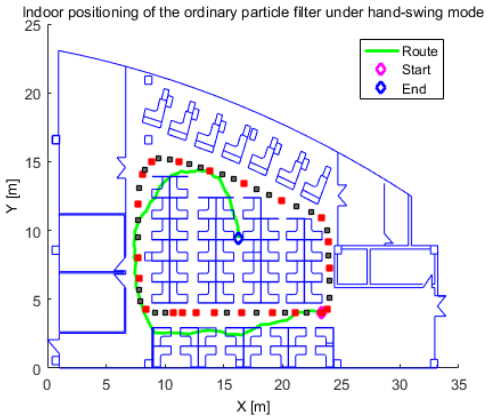

FIGURE 27. Indoor positioning result of the ordinary particle filter under hand-swing mode.

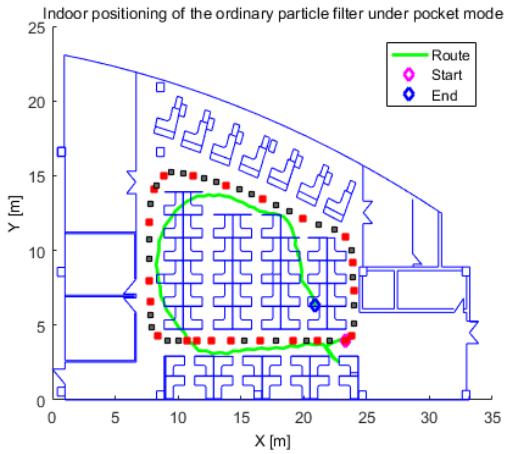

FIGURE 28. Indoor positioning result of the ordinary particle filter under pocket mode.

Fig.27 and Fig.28 shows the OPF positioning results of under hand-swing mode and pocket mode respectively. We can see that the increasing heading estimation error results in the positioning failure because the OPF cannot make a stable and robust heading estimation when the carrying mode changes. The final positioning errors of three filters are shown in Table 5.

TABLE 5. The table of indoor positioning error of heading estimation assistance.

Item	67th Error Percentile	95th Error Percentile
MPF	0.54m	0.89m
OPF	0.58m	1.24m
KF	1.52m	3.40m

Furthermore, we carried out the heading estimation optimization test based on multidimensional particle filter. The heading estimation and positioning result is shown in Fig.29.

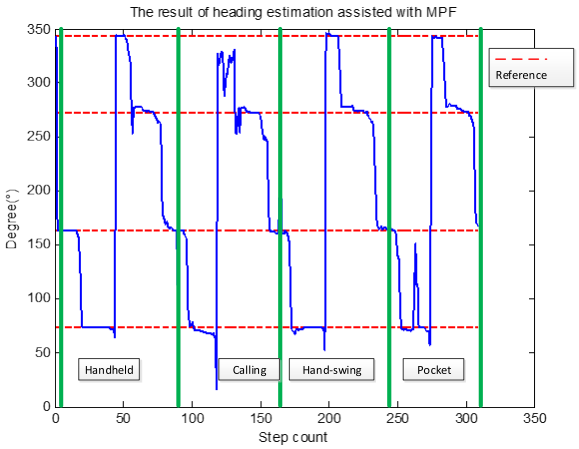

FIGURE 29. The result of heading estimation assisted with MPF. The red dashed lines show the reference heading of the test path shown in Fig.24 (a).

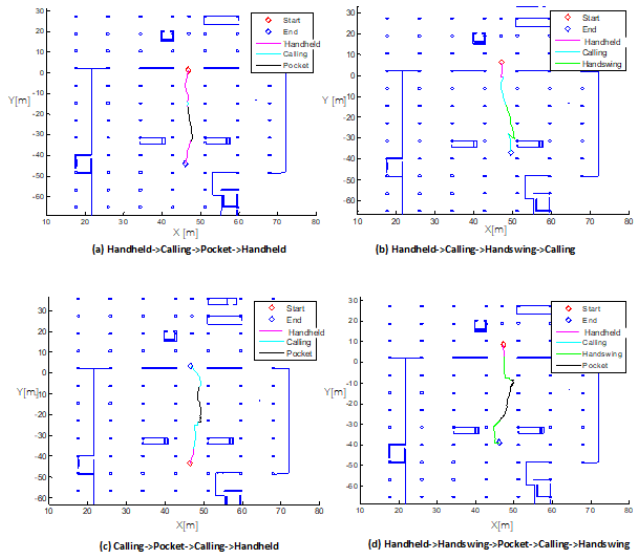

FIGURE 30. Underground car park tests with smartphone carrying mode causally changed. (a) Handheld->Calling->Pocket->Handheld. (b) Handheld->Calling->Handswing->Calling. (c) Calling->Pocket->Calling->Handheld. (d) Handheld->Handswing->Pocket->Calling->Handswing.

Last, we carried out challenging tests in an underground car park with 7200m^2 using a SAMSUNG Galaxy S6 (Android 6.0.1) to verify the performance of proposed solution in a sparse map constraint environment. The magnetic field of this car park is still suffered from dense concrete pillars and full occupied vehicles. A user walked along a straight line with 45 meters while smartphone carrying mode was causally changed among four carrying modes as shown in Fig. 30. Four test cases show that the proposed solution can handle the scenario of carrying mode change. The transform from/to the hand-swing mode introduces more errors compared to other transforms. Results show that the average error of positioning is less than 2.5 meters with MPF even though in the map-less environment.

IV. CONCLUSION

This research paper proposes algorithms focusing on heading estimation and its optimization application on a smartphone platform. The proposed algorithm and suggested magnetometer calibration process can eliminate the influence of magnetic interference in a certain indoor environment range. The heading estimation algorithm using acceleration information makes it possible to achieve accurate heading estimation in different carrying modes and enables various random smartphone handling modes for indoor positioning pedestrians LBS. Moreover, combined with road constraints information, the heading estimation during positioning can correct the heading error effectively. Finally, this paper presents a multidimensional particle filter scheme that combines PDR and motion recognition, which improves positioning accuracy and robustness in addition to optimizing the heading estimation as well. The experimental results show a good performance in both positioning and heading estimation.

The challenging tests present a decreased performance. In future, we will introduce the WiFi, Bluetooth, and magnetic field fingerprints into the MPF to achieve a more practical smartphone-based indoor positioning approach. In addition, the more complex carrying mode such as bag mode and more types of smartphone will be further investigated.

REFERENCES

[1] (Jun. 6, 2018). *Google Project Tango*. [Online]. Available: http://www.google.com/atap/project-tango/
[2] M. Serino, K. Cordrey, R. L. Milanaik, and L. McLaughlin, "Pokémon Go and augmented virtual reality games: A cautionary commentary for parents and pediatricians," *Current Opinion Pediatrics*, vol. 28, no. 5, pp. 673–677, 2016.
[3] R. Mautz, "Indoor positioning technologies," Ph.D. dissertation, Dept. CEGE, ETH Zürich, Zürich, Switzerland, 2012.
[4] H. Ju, S. Y. Park, and C. G. Park, "A smartphone-based pedestrian dead reckoning system with multiple virtual tracking for indoor navigation," *IEEE Sensors J.*, vol. 18, no. 16, pp. 6756–6764, Aug. 2018.
[5] J. M. Loomis, R. L. Klatzky, R. G. Golledge, and J. W. Philbeck, "Human navigation by path integration," in *Wayfinding Behavior: Cognitive Mapping and Other Spatial Processes*. Baltimore, MD, USA: The Johns Hopkins Univ. Press, 1999, pp. 125–151.
[6] Q. Ladetto, "On foot navigation: Continuous step calibration using both complementary recursive prediction and adaptive Kalman filtering," in *Proc. ION GPS*, Sep. 2000, pp. 1735–1740.
[7] E. Foxlin, "Pedestrian tracking with shoe-mounted inertial sensors," *IEEE Comput. Graph. Appl.*, vol. 25, no. 6, pp. 38–46, Nov./Dec. 2005.
[8] P. Bahl and V. N. Padmanabhan, "RADAR: An in-building RF-based user location and tracking system," in *Proc. IEEE 19th Annu. Joint Conf. Comput. Commun. Societies (INFOCOM)*, vol. 2, Mar. 2000, pp. 775–784.
[9] J. Hallberg, M. Nilsson, and K. Synnes, "Positioning with Bluetooth," in *Proc. IEEE 10th Int. Conf. Telecommun. (ICT)*, vol. 2, Feb./Mar. 2003, pp. 954–958.
[10] W. F. Storms, "Magnetic field aided indoor navigation," Graduate School Eng. Manage., Air Force Inst. Technol., Wright-Patterson Air Force Base, OH, USA, Tech. Rep. AFIT/GE/ENG/09-44, 2009.
[11] A. Mulloni, D. Wagner, I. Barakonyi, and D. Schmalstieg, "Indoor positioning and navigation with camera phones," *IEEE Pervasive Comput.*, vol. 8, no. 2, pp. 22–31, Apr. 2009.
[12] J. W. Kim, H. J. Jang, D.-H. Hwang, and C. Park, "A step, stride and heading determination for the pedestrian navigation system," *Positioning*, vol. 1, no. 8, pp. 273–279, 2004.
[13] X. Yuan, S. Yu, S. Zhang, G. Wang, and S. Liu, "Quaternion-based unscented Kalman filter for accurate indoor heading estimation using wearable multi-sensor system," *Sensors*, vol. 15, no. 5, p. 10872, 2015.

[14] A. Motwani, W. Liu, R. Sutton, R. Bucknall, and S. Sharma, "An interval Kalman filter–based fuzzy multi-sensor fusion approach for fault-tolerant heading estimation of an autonomous surface vehicle," *Proc. Inst. Mech. Eng. M, J. Eng. Maritime Environ.*, vol. 230, no. 3, pp. 491–507, 2016.

[15] W. Chen, R. Chen, H. Kuusniemi, J. Wang, and Y. Chen, "An effective pedestrian dead reckoning algorithm using a unified heading error model," in *Proc. IEEE Position Location Navigat. Symp.*, May 2010, pp. 340–347.

[16] W. Kang and Y. Han, "SmartPDR: Smartphone-based pedestrian dead reckoning for indoor localization," *IEEE Sensors J.*, vol. 15, no. 5, pp. 2906–2916, May 2015.

[17] W. Kang, S. Nam, S. Lee, and Y. Han, "Improved heading estimation for smartphone-based indoor positioning systems," in *Proc. IEEE Int. Symp. Pers. Indoor Mobile Radio Commun.*, Sep. 2012, pp. 2449–2453.

[18] U. Blanke and B. Schiele, "Sensing location in the pocket," *Quart. J. Exp. Psychol.*, vol. 19, no. 1, pp. 54–58, 2008.

[19] U. Steinhoff and S. Schiele, "Dead reckoning from the pocket—An experimental study," in *Proc. IEEE Int. Conf. Pervasive Comput. Commun.*, Mar./Apr. 2010, pp. 162–170.

[20] K. Kai, P. Lukowicz, B. Begole, and K. Partridge, "Which way am I facing: Inferring horizontal device orientation from an accelerometer signal," in *Proc. IEEE Int. Symp. Wearable Comput.*, Sep. 2009, pp. 149–150.

[21] Z.-A. Deng, G. Wang, Y. Hu, and D. Wu, "Heading estimation for indoor pedestrian navigation using a smartphone in the pocket," *Sensors*, vol. 15, no. 9, pp. 21518–21536, 2015.

[22] Z. Deng, X. Liu, Z. Qu, C. Hou, and W. Si, "Robust heading estimation for indoor pedestrian navigation using unconstrained smartphones," *Wireless Commun. Mobile Comput.*. vol. 2018, Jul. 2018, Art. no. 5607036.

[23] Z. Xiao, H. Wen, N. Trigoni, and A. Markham, "Robust pedestrian dead reckoning (R-PDR) for arbitrary mobile device placement," in *Proc. IEEE Int. Conf. Indoor Positioning Indoor Navigat.*, Oct. 2015, pp. 187–196.

[24] S. Qiu, Z. Wang, H. Zhao, K. Qin, Z. Li, and H. Hu, "Inertial/magnetic sensors based pedestrian dead reckoning by means of multi-sensor fusion," *Inf. Fusion*, vol. 39, pp. 108–119, Jan. 2018.

[25] Y. Li, Y. Zhuang, P. Zhang, H. Lan, X. Niu, and N. El-Sheimy, "An improved inertial/WiFi/magnetic fusion structure for indoor navigation," *Inf. Fusion*, vol. 34, pp. 101–119, Mar. 2017.

[26] R. Harle, "A survey of indoor inertial positioning systems for pedestrians," *IEEE Commun. Surveys Tuts.*, vol. 15, no. 3, pp. 1281–1293, 3rd Quart., 2013.

[27] W. Kwon, K.-S. Roh, and H.-K. Sung, "Particle filter-based heading estimation using magnetic compasses for mobile robot navigation," in *Proc. IEEE Int. Conf. Robot. Automat.*, May 2006, pp. 2705–2712.

[28] (Jun. 6, 2018). *Calibrate Your Compass: Figure 8 Pattern Method*. [Online]. Available: https://calibratecompass.com/

[29] L. Wang *et al.*, "A robust context-based heading estimation algorithm for pedestrian using a smartphone," in *Proc. 28th Int. Tech. Meeting Satell. Division Inst. Navigat. (ION GNSS)*, Tampa, FL, USA, Sep. 2015, pp. 2493–2500 .

[30] M. Chao, D. Jiang, and C. Wen, "Error analysis and calibration of magnetic compass," *Chin. J. Sens. Actuators*, vol. 23, no. 4, p. 018, 2010.

[31] M. H. Afzal, "Use of Earth's magnetic field for pedestrian navigation," Ph.D. dissertation, Dept. Geomatics Eng., Univ. Calgary, Calgary, AB, Canada, 2011.

[32] M. H. Afzal, V. Renaudin, and G. Lachapelle, "Magnetic field based heading estimation for pedestrian navigation environments," in *Proc. Int. Conf. IEEE Indoor Positioning Indoor Navigat. (IPIN)*, Sep. 2011, pp. 1–10.

[33] J. M. G. Merayo, P. Brauer, F. Primdahl, J. R. Petersen, and O. V. Nielsen, "Scalar calibration of vector magnetometers," *Meas. Sci. Technol.*, vol. 11, no. 2, pp. 120–132, 2000.

[34] J. Fang, H. Sun, X. Zhang, Y. Tao, and J. Cao, "A novel calibration method of magnetic compass based on ellipsoid fitting," *IEEE Trans. Instrum. Meas.*, vol. 60, no. 6, pp. 2053–2061, Jun. 2011.

[35] T. Ozyagcilar, "Calibrating an ecompass in the presence of hard and soft-iron interference," in *Proc. Freescale Semiconductor*, 2012, pp. 1–17.

[36] D. Liu *et al.*, "Simplified ellipsoid fitting-based magnetometer calibration for pedestrian dead reckoning," in *Proc. China Satell. Navigat. Conf. (CSNC)*, vol. 2. Singapore: Springer, 2016, pp. 473–486.

[37] J. Qian, L. Pei, R. Ying, P. Liu, and J. Ma, "Vector graph assisted pedestrian dead reckoning using an unconstrained smartphone," *Sensors*, vol. 15, no. 3, pp. 5032–5057, 2015.

[38] S. O.H. Madgwick, "An efficient orientation filter for inertial and inertial/magnetic sensor arrays," Dept. Mech. Eng., Univ. Bristol, Bristol, U.K., Tech. Rep., Apr. 2010, pp. 113–118.

[39] D. Liu *et al.*, "A novel heading estimation algorithm for pedestrian using a smartphone without attitude constraints," in *Proc. 4th Int. Conf. Ubiquitous Positioning, Indoor Navigat. Location Based Services (UPINLBS)*, 2016, pp. 29–37.

[40] A. Perttula, H. Leppäkoski, M. Kirkko-Jaakkola, P. Davidson, J. Collin, and J. Takala, "Distributed indoor positioning system with inertial measurements and map matching," *IEEE Trans. Instrum. Meas.*, vol. 63, no. 11, pp. 2682–2695, Nov. 2014.

[41] H. Shin, Y. Chon, and H. Cha, "Unsupervised construction of an indoor floor plan using a smartphone," *IEEE Trans. Syst., Man, Cybern. C, Appl. Rev.*, vol. 42, no. 6, pp. 889–898, Nov. 2012.

[42] K. Abdulrahim, C. Hide, T. Moore, and C. Hill, "Integrating low cost IMU with building heading in indoor pedestrian navigation," *J. Global Positioning Syst.*, vol. 10, no. 1, pp. 30–38, 2011.

[43] J. A. B. Link, P. Smith, N. Viol, and K. Wehrle, "Footpath: Accurate map-based indoor navigation using smartphones," in *Proc. IEEE Int. Conf. Indoor Positioning Indoor Navigat. (IPIN)*, Sep. 2011, pp. 1–8.

[44] J. Yang and R. S. Wang, "Classified road detection from satellite images based on perceptual organization," *Int. J. Remote Sens.*, vol. 28, no. 20, pp. 4653–4669, 2007.

[45] Y. Rianto, T. Kim, and S. Kondo, "Detection of roads from satellite image using the optimal search," in *Proc. IEEE Asia–Pacific Conf. Circuits Syst. (APCCAS)*, Sep. 2000, pp. 587–590.

[46] F. Ameri, A. M. Mobaraki, and M. J. V. Zoej, "Semi-automatic extraction of different-shaped road centerlines from MS and pan-sharped IKONOS images," *Proc. 21st ISPRS Congr.ăTech. Commission III*, Beijing, China, 2008, pp. 621–626.

[47] S. Beauregard, Widyawan, and M. Klepal, "Indoor PDR performance enhancement using minimal map information and particle filters," in *Proc. IEEE/ION Position, Location Navigat. Symp.*, May 2008, pp. 141–147.

[48] A. Doucet and A. M. A. Johansen, "Tutorial on particle filtering and smoothing: Fifteen years later," in *The Oxford Handbook of Nonlinear Filtering*. Oxford, U.K.: Oxford Univ. Press, 2011.

[49] L. M. Murray, A. Lee, and P. E. Jacob. (2013). "Rethinking resampling in the particle filter on graphics processing units." [Online]. Available: https://arxiv.org/abs/1301.4019v1

[50] F. Antonio, "Faster line segment intersection," in *Graphics Gems III*. New York, NY, USA: Academic, 1992, pp. 199–202.

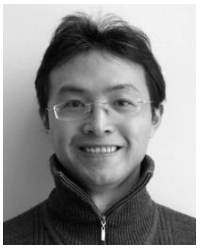

LING PEI received the Ph.D. degree from Southeast University, Nanjing, China, in 2007. From 2007 to 2013, he was a Specialist Research Scientist with the Finnish Geospatial Research Institute. He is currently an Associate Professor with the School of Electronic Information and Electrical Engineering, Shanghai Jiao Tong University. He has authored or co-authored over 90 scientific papers. He holds 24 patents and pending patents. His main research is in the areas of indoor/outdoor seamless positioning, ubiquitous computing, wireless positioning, bio-inspired navigation, context-aware applications, location-based services, and navigation of unmanned systems. He was a recipient of the Shanghai Pujiang Talent in 2014.

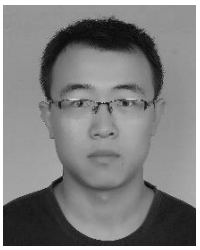

DONGHUI LIU received the B.S. degree in electrical engineering from Shanghai Jiao Tong University, Shanghai, China, in 2016, where he is currently pursuing the master's degree with the Shanghai Key Laboratory of Navigation and Location-Based Services. His main research is in the areas of indoor/outdoor seamless positioning, ubiquitous computing, wireless positioning, and pedestrian dead reckoning. He was a recipient of the Best Youth Talent Paper Award of CSNC 2016.

DANPING ZOU received the B.S. degree from the Huazhong University of Science and Technology, Wuhan, China, and the Ph.D. degree from Fudan University, Shanghai, China, in 2003 and 2010, respectively. From 2010 to 2013, he was a Research Fellow with the Department of Electrical and Computer Engineering, National University of Singapore, Singapore. In 2013, he joined the Department of Electronic Engineering, Shanghai Jiao Tong University, Shanghai, as an Associate Professor. His research interests include low-level 3-D vision on robotics.

RONALD LEE FOOK CHOY received the B.S. degree in electrical engineering from McGill University, Montreal, Canada, in 2003. He is currently the Machine Learning Test Director with the Shanghai BeiDou Research Institute, with responsibilities to build the biggest robotics test and training facility in China. His research focuses on benchmarking autonomous machines performance based on GNC applications with a special interest on stereo vision, ToF vision, LiDAR vision, and data fusion to achieve indoor/outdoor positioning and navigation.

YUWEI CHEN received the B.E. and M.Sc. degrees from the Department of Information Science and Electronics Engineering, Zhejiang University, China, in 1999 and 2002, respectively, and the Ph.D. degree in circuits and systems from the Shanghai Institute of Technical Physics, Chinese Academy of Sciences, in 2005. He is currently with the Finnish Geospatial Research Institute as a Research Manager leading the research group Remote Sensing Electronics, which focuses on developing new remote sensing systems. He is also a Guest Professor of the Academy of Opto-Electronics, Chinese Academy of Sciences. He holds 10 patents. He has authored and co-authored over 100 scientific papers and book chapters. His research interests include LiDAR, hyperspectral LiDAR, radars, and navigation and positioning.

ZHE HE received the B.S. and M.S. degrees in navigation guidance and control from Shanghai Jiao Tong University, and the Ph.D. degree in geomatics engineering from the University of Calgary, Canada. He was a Post-Doctoral Fellow with the Position, Location and Navigation Group, Department of Geomatics Engineering, University of Calgary. He is currently the Director of technology of Appropolis Inc., Calgary, focusing on LPWAN and LBS. His research interests are statistical estimation theory applied to GNSS, inertial and integrated navigation systems, and low-power wide area network LBS systems.